TECHNICAL NOTE

# DETERMINATION OF WHOLE FIELD STRAIN IN COMPOSITE REFLECTOR USING PHOTOGRAMMETRY

Vivek Prabhakar, K. Renji, Raghunatha Behara
Structures Group
ISRO Satellite Centre (ISAC)
Old Airport Road, Kodihalli
Bangalore-560 017, India
Email : renji@isac.gov.in

**Abstract**

*Conventional strain measurement techniques cannot be used to obtain the strains in composite reflectors under thermal environment. Though photogrammetry can be used to measure the deformations it cannot provide information on strains. In this work a methodology is developed to determine the strains from the displacements obtained from photogrammetry coordinate measurement. The strains are determined by applying equilibrium conditions and not from the gradient of the displacements. The results are verified using simulated data as well as experiment. It is demonstrated for a composite reflector of a typical spacecraft when subjected to thermal load. The methodology developed in this work helps in obtaining the strain distribution without using expensive digital image correlation equipment. This methodology can be used on wide variety of applications like inflatable structures, flexible structures etc., where strain gauge measurements are not possible to be carried out.*

***Keywords****: Photogrammetry, Strain, Non-destructive Evaluation, Finite Element Analysis, Composite Reflector*

## Introduction

Stability of the surface shape of reflectors under space environment is very essential in communication satellites. These are often specified by the RMS value of the deviations from the desired surface [1, 2]. The specifications are more stringent for Ku or Ka band antenna. Therefore most of these reflectors are made of composite materials. They are generally made with CFRP or Kevlar face sheets with honeycomb core. Though some portion of the reflector is covered with multi-layer insulation, the radiating surfaces of the reflectors are exposed to extreme space environment. These temperature variations cause the reflecting surface to deform causing degradation in the performance [3, 4].

The deformations under thermal environment are verified through a test is thermo-vacuum chamber and the deformations are measured using a non-contact measurement technique. In the recent past photogrammetry has become an important tool for non-contact and whole field coordinate measurement [5, 6]. In photogrammetry a number of photographs of the object are taken from different positions and orientations of the camera and these photographs are analysed to obtain the coordinates of points on the surface of three dimensional bodies [6, 7]. In this technique it is not necessary to have the precise location of the camera for each photograph.

Though photogrammetry can provide information on the coordinate as well as displacement, it does not provide information on strains. Use of conventional strain gauging technique has several issues while using for this application. The strains gauges cannot be mounted on the radiating surface of the reflector. Use of strain gauges in thermo-vacuum chamber and correction of the measured strains to obtain the actual strain is another issue. Also, it does not do a whole field measurement. On thin membranes, in some other applications, the strain gauges cannot be mounted.

Jin et al. [8] used Digital Image Correlation (DIC) technique for such an application. They obtained thermal

**Paper Code : V69 N2/953-2017**. Manuscript received on 28 Jul 2016. Reviewed and accepted as a Technical Note on 11 Apr 2017

deformation and thermal buckling behaviour of a laminated composite plate in a titanium ring using the DIC technique [8]. For the above experiment the test article has to be painted with DIC paint. This paint is not allowed for most of the space grade reflectors. Out-gassing is another major problem. Also, one should have the costly DIC equipment.

In this work a methodology is developed in extracting the strains from the known (measured) displacements which overcomes the above discussed limitations. There are several attempts reported in the usage of displacement data in extracting the strains [5, 9]. In those works, as late as 2012 [9], the strains are obtained as gradients of the displacements. That is, the displacements at the known points are taken and then a gradient of these displacements with respect to the distance is taken as the strain. This way of determining strains from the known displacements has several limitations. These are explained later.

In the present work the strains are not extracted through a simple calculation of difference in displacement over the displacement grid length, instead they are computed by applying equilibrium conditions. A FE like mesh is created. Since the equilibrium equations are formed without the information on the actual structural properties investigations are also carried out on the influence of these parameters on the extracted strains. As rotational displacements are not directly available in photogrammetric measurements the strains are extracted without these displacements. Sensitivity of the rotational displacements on the strains determined is also explored. Finally the methodology developed is validated by simulated data as well as by experiments.

It is to be emphasized here that the FE model of the structure is not available and strains are obtained from the displacements without using the actual FE model. Though it is mentioned as photogrammetry data, it can be any set of displacement data. Since photogrammetry is very commonly used for obtaining the displacement, the phrase displacement from photogrammetry data is used in this work. The present work is carried out on a reflector. One does not expect the strains obtained using this methodology to be exactly equal to the strains measured using a strain gauge. This is because the strain gauge gives the strain as an average in a small region of gauge length which is typically about 2 mm, whereas the spacing of photogrammetry target will be considerably higher. But it can be seen that using the proposed methodology strains close to those measured by strain gauges can be obtained.

## Displacement Measurements on the Composite Antenna Reflector

Reflector of a typical communication satellite (Fig.1) is tested in thermo-vacuum chamber [10]. Deformations caused due to the temperature variations are measured using photogrammetry. Fig.1 and 2 shows the experimental set-up and test specimen with PG targets. Retro reflective targets at a spacing of around 20-30 mm are used (Fig.2). 8 Mega pixel resolution digital camera is used for the experiment. The camera has an on-board processor to do image processing such as identification of the coded targets detected and estimation of camera intrinsic and extrinsic parameters. Photogrammetry software is used to compute the 3D positions of the retro reflective targets mounted on the object. The centroid of each circular target is extracted. These pixel coordinates are the input elements for a photogrammetric bundle adjustment which provides 3D reconstruction and the camera position and attitude [11, 12]. Based on the 3D positions of un-deformed and the deformed structure, the displacements are computed.

The accuracy of the camera has a fixed component of 5 microns in addition to 5 microns for every meter size of the test article. The measurement uncertainty is known to vary linearly as the size of the test object. The length of the test article is 2.2 m. The expected maximum error is less than 20 microns.

## Methodology for Determination of Strains

### Strain Displacement Relations

From the basic principles of physics, it is known that the strain is the change in dimension to the original dimension [13]. The causes of strain can be Mechanical loads (forces, pressures, etc.) or Temperature change (thermal expansion). A point P(x, y, z) moves to P(x+u, y+v, z+w), where the displacement components are functions of position:

$u = u(x, y, z)$, $v = v(x, y, z)$, $w = w(x, y, z)$

At P consider an infinitesimal rectangle PQRS (Fig.3) of side lengths $\{dx, dy\}$ aligned with the axes $\{x, y\}$. The square maps to a quadrilateral P' Q' R' S in the deformed body.

The average strain components are taken over a finite portion of the body; for example using a strain gage. The strains can be computed from the known displacement values.

$$\varepsilon_{x,\,x,\,average} = \frac{\Delta u}{\Delta x} \quad (1)$$

$$\varepsilon_{y,\,y,\,average} = \frac{\Delta v}{\Delta y} \quad (2)$$

$$\varepsilon_{x,\,y,\,average} = \frac{\Delta v}{\Delta x} + \frac{\Delta u}{\Delta y} \quad (3)$$

**Conventional Strain Computation**

The simplest method of calculating strains from displacement is to substitute the displacements in the Eqs.1-3. In order to account for all the strain components including the shear strain, 4 segments have to be calculated per a rectangular element. For a 40x40 target configuration around 6400 line segments need to be computed. Hand calculation will be cumbersome, and hence one can use a computer program to do the above calculation. Even though the magnitude of the direct strains can be calculated using the above equations, visualization of the strain pattern will not be possible. The strains are obtained only at the displacement measurement locations, as in the case of strain gauge. Therefore the accuracy will depend on the spacing of the locations at which the displacements are known. The strains in the region between two such locations can only have linear variations which will not be correct when the spacing is large.

**Improved Method**

An improved method is proposed here. In this method a finite element type mesh is created and the known displacements are enforced at the nodes where the photogrammetric measurements are carried out. A static analysis is carried out using this model and the strains are computed. It is to be noted that no real finite element model is used, instead only a finite element type mesh is required, i.e., actual structural and material properties are not required. This aspect is discussed later.

**Surface Re-construction and Generation of Finite Element Type Mesh**

A photogrammetry (PG) measurement gives the point cloud data in (x, y, z) coordinates and this photogrammetric data form the basis for the strain estimation. First the surface re-construction is carried out with initial PG data (Z0). For surface construction triangulation method is used. While there are numerous algorithms for computing triangulations, it is the favourable geometric properties of the Delaunay triangulation that makes it so useful. Delaunay triangulation gives proper triangular elements without ill-conditioned elements which makes the mesh suitable for further usage in Finite element method. In mathematics and computational geometry, a Delaunay triangulation for a set of points in a plane is a triangulation such that no point is inside the circum-circle of any triangle [14]. Delaunay triangulations maximize the minimum angle among all the internal angles of the triangles in the triangulation. This will create a C0 surface which has displacement continuity at the edges.

In the present study, since the article is in a 3D domain, first the triangulation is carried out in a 2D plane and the third coordinate is enforced on the triangulation points to get the 3D surface. Then the generation of the Finite Element Type Mesh is carried out. The point location is exported as node and the triangle connectivity is exported as element. This will be the reference shape for the analysis (Z0). A Finite Element mesh is created from the photogrammetric data (Fig.4). Fig.5 shows the deformed pattern.

**Application of Displacement**

Measured displacements obtained from the initial cloud data Z0 (X, Y, Z) and the deformed data Z1 (X, Y, Z) of Photogrammetry. These displacements are applied to the respective nodes as enforced displacement. A MATLAB code converts these data into a NASTRAN solver file and is then solved using NASTRAN or any basic finite element software as a static analysis.

**Strains from Enforced Displacements**

Consider the equilibrium equations,

$$[\,K\,]\{\,U\,\} = \{\,F\,\} \quad (4)$$

where [K] is the global stiffness matrix, $\{U\}$ is the vector of computed node displacements. In this case, first these matrices are partitioned into two separate matrices, one with enforced displacement degree of freedom and the other has the rest of the degree-of-freedom.With the matrix with the enforced displacements, the associated forces $\{F_{enf}\}$ will be solved. Using these forces in the other partitioned matrix the remaining displacements are solved.

$$[\,K\,]\{\,U\,\} = \{\,F\,\}$$

[ K ] = Global stiffness matrix

{ U } = Displacement matrix
{ F } = Equivalent nodal forces

The unknown is the force required to enforce displacement.

$$[K]\{U_{enf}\} = \{F_{enf}\} \quad (5)$$

$$\{U\} = [K]-1\{F_{mod}\} \quad (6)$$

Now we have all displacements and the forces that result in the enforced displacement. From these displacements, the strains {e} in the element are calculated using the equation,

$$\{e\} = [B]\{U\} \quad (7)$$

where B is the strain-displacement matrix and U is the vector of computed element node displacements.

**Structural Properties**

In this methodology some typical values, not the actual values, of the structural properties are assigned and the strains are computed. To carry out the computation using FE method, the material properties and the cross section properties need to be assigned to the elements. When FE model is used to determine strains from enforced displacements it is known that the strains do not depend on the structural properties. In the method developed here the strains are determined without using the actual FE model, meaning that the cross-sectional and material properties are unknown. However the influence of the structural properties on the extracted strain is verified and presented later.

Using the method developed here only the surface strains are obtained and the variation of strain along *z* direction is not captured, which is the case with any measurement technique. Here the mid-plane strains in the model correspond to the surface strains of the object. Since the modulii of elasticity of the material are not known, the stresses cannot be calculated from the strains.

Strains are calculated using the proposed technique from the photogrammetric coordinate data and shown in Fig.6, 7. In the absence of proposed technique, the whole field strains would not have been obtained from the thermo-vac measurement.

**Validation of the Technique**

Initially, the validation is done using a finite element model. A cylindrical shell of 2m diameter is idealized. In order to create a non-uniform strain distribution an embedded block is incorporated. The base of the cylinder is fixed and axial compressive load is applied as shown in Fig.8. QUAD4 element with 20 mm mesh size is used to model the cylinder. MSC Nastran is used for the analysis. Finite element mesh is shown in the Fig.8. The displacement plot is shown in the Fig.9. The strain in the X and Y direction are shown in Fig.10. These results are taken as reference strain values. Table-1 gives the maximum strain values. The results are plotted such that the Y direction corresponds to the Cylinder longitudinal and X direction corresponds to the Cylinder circumferential direction. Fig.11 shows the result in the visibility area. The displacement in this area is used as input data for determining the strain field using the method developed here.

The computed displacement (T1, T2, T3) can be thought as displacement measured using photogrammetry. From these displacements, the strains are obtained using the proposed method. First, the displacements are computed with a mesh size of 80 mm. This means the displacements are available for a photogrammetric target spacing of 80 mm. A FE type mesh is created using the coordinate data (Fig.13). Some typical properties, not the actual properties, have been assigned for the elements. Previously computed displacements are enforced at the nodes and the strains are computed. All the three components of the deformation are used. The strains computed from the displacements using the proposed method are given in Fig.12 and Table-2. The results show that these are in very good agreement with the actual strains (computed using actual FE model).

**Table-1 : Strains for Different Values of Moduli**

| | | High Modulus | | | Low Modulus | | |
|---|---|---|---|---|---|---|---|
| Location | Element ID | $\varepsilon_x$ | $\varepsilon_y$ | $\tau_{xy}$ | $\varepsilon_x$ | $\varepsilon_y$ | $\tau_{xy}$ |
| Location 1 | 2 | -1.024E-03 | -1.001E-03 | -3.664E-03 | -1.024E-03 | -1.001E-03 | -3.664E-03 |
| Location 2 | 12 | -1.002E-03 | -9.701E-04 | -3.721E-03 | -1.002E-03 | -9.701E-04 | -3.721E-03 |

It is well known that when a FE model is used to determine the strains with known displacements as the boundary conditions, the strains do not depend on the material property. The same result is expected while using the proposed method. This aspect, though expected, is demonstrated here. Two iterations are carried out, one with a high modulus of elasticity (E) and the second has a low modulus of elasticity. The ratio of the modulus value is 1000. The table given shows the comparison of the results. Few elements are taken for comparison. It can be seen that as expected the strain values are insensitive to the modulus values.

The photogrammetric data provides the displacements. Therefore the strains are obtained enforcing the displacements but without enforcing the rotations. When FE model is used to determine strains from enforced displacements it is known that strains can be determined by enforcing displacements alone and the rotations need not be known and the same is expected while using the present method. This aspect, though expected, is demonstrated here. The results of the cylinder loaded in compression described previously are used for the study. First the strains are obtained using the finite element model. Also, the translations and rotations are extracted. Only the translation values are applied in the Finite element model. Later both translations as well as rotations are enforced. The results are given in Table-2. Results are given without considering the edge elements.

The strain values are identical regardless of whether the rotations are imposed or not. This means that the computed strain values are not affected by the rotation values at the PG target locations. It can be seen that the strains in the normal direction as well as the shear are same. These results are also same as the results obtained using the actual finite element model.

**Effect of Target Spacing on the Estimated Strain**

In order to obtain the influence of target spacing, the strains are determined with displacements enforced at nodes with various spacing. These results are compared with the results of the finite element which are with a mesh size of 20 mm. The results are given in Table-3 for 3 regions in the structure, viz., on the cylinder, on the block and on the transition zone. In general, as the node/target spacing increases, the deviation from the finite element result increases and the maximum strain values are reduced as the target spacing is increased. In the region where the strain is uniform, the variation is around 2%. Maximum deviation is found in the transition zone. In this

**Table-2 : Comparison of Strains with and without Rotation Values**

| | Strain with Translation Values | | | Strain with translation and Rotation | | |
|---|---|---|---|---|---|---|
| Element ID | $\varepsilon_x$ | $\varepsilon_y$ | $\tau_{xy}$ | $\varepsilon_x$ | $\varepsilon_y$ | $\tau_{xy}$ |
| 91 | -2.5133E-05 | -1.1986E-03 | 2.1410E-03 | -2.5118E-05 | -1.1986E-03 | 2.1409E-03 |
| 92 | 3.8151E-04 | -2.7000E-03 | 1.4230E-05 | 3.8151E-04 | -2.7000E-03 | 1.4230E-05 |
| 93 | 3.7162E-04 | -2.7000E-03 | 1.1789E-05 | 3.7162E-04 | -2.7000E-03 | 1.1789E-05 |
| 94 | 3.8457E-04 | -2.7000E-03 | 3.5346E-06 | 3.8457E-04 | -2.7000E-03 | 3.5346E-06 |

**Table-3 : Strains Determined with Different Values of Target Spacing**

| | On the Block | | On the Cylinder | | Between the Block and the Cylinder | |
|---|---|---|---|---|---|---|
| | $\varepsilon_x$ | $\varepsilon_y$ | $\varepsilon_x$ | $\varepsilon_y$ | $\varepsilon_x$ | $\varepsilon_y$ |
| FELL FEM | 5.11E-04 | -1.63E-03 | 9.09E-04 | -2.95E-03 | 6.64E-04 | -2.48E-03 |
| MESH_40mm | 5.11E-04 | -1.63E-03 | 9.09E-04 | -2.95E-03 | 6.64E-04 | -2.48E-03 |
| MESH_80mm | 5.11E-04 | -1.65E-03 | 9.06E-04 | -2.96E-03 | 6.80E-04 | -2.43E-03 |
| MESH_120mm | 5.22E-04 | -1.65E-03 | 9.08E-04 | -2.94E-03 | 6.84E-04 | -2.42E-03 |
| MESH_160mm | 5.43E-04 | -1.68E-03 | 8.82E-04 | -2.95E-03 | 7.00E-04 | -2.44E-03 |

zone, even with a spacing of 80 mm (Fig.14), the strains determined are within 3% of the finite element results. Therefore target spacing of even 80 mm can provide the strains with reasonable accuracy, provided there are no sudden introductions of load.

### Experimental Validation

Experiments are conducted to validate the proposed estimation technique. In the case of antenna reflector, it was not possible to have the strain gauges mounted. Therefore a typical sandwich panel is loaded statically and the strains are measured. Photogrammetric measurements are carried out to obtain the displacements. From the PG data, strains are computed and compared with the measured strains. The test setup is shown in Fig.15a. The dimensions of the specimen are 150mm x 250mm. Strain gauges are mounted at 7 discrete locations on the outer surface of the specimen as shown in Fig.15b. The gauge length of the strain gauge is 2mm and the measured strain can be interpreted as an average over 2mm. On the outer surface of the specimen photogrammetric target are also mounted. There are 35 targets for this purpose. The spacing of the targets is approximately 20mm.

Initial coordinates are measured using photogrammetry. Load is applied using a 5T capacity Universal testing machine at a rate of 0.5mm/min. Photogrammetry measurements are taken again at the loaded condition. Loading is paused at the time of measurement. The coordinates are measured by using a single camera but taken from multiple locations and orientations. Since it is a static deformation, it is equivalent to having several cameras. Three cameras are sufficient to describe the location of a point in 3D space. In this case 30 photos are taken using INCA3A camera having a resolution of 8 Mega pixels. Data is processed using V-Stars software. Strains are measured at the identified locations using strain gauges. The strains measured at various locations during static test are given in Table-4.

Finite Element mesh (Fig.16a) is created from photogrammetric data. The deformed pattern obtained using PG is shown in Fig.16b. From the photogrammetric coordinate measurement data, the strains are obtained using the proposed technique and given in Fig.17 and at few locations corresponding to measurement locations are given in Table-5. A comparison of the measured strain and the strain derived using the photogrammetry data is also given in Table-5. It is seen that the strains obtained using the proposed technique are close (about 12%) to the measured strains. Thus, it is seen that with a very reasonable accuracy the strains can be obtained using the proposed technique.

### Summary and Conclusions

A methodology to estimate the strains from the measured displacements is developed. In conjunction with the measured displacements, it uses a finite element type model and the strains are obtained by enforcing the measured displacements. To determine the strains using this methodology the actual finite element model is not required. The technique is validated through the results of finite element method. It has been demonstrated that one can determine the strains with sufficient accuracy even

**Table-4 : Strains Measured (με) During Static Load Test**

| Load (N) | Strain Gauge Location | | | | | | |
|---|---|---|---|---|---|---|---|
| | 1 | 2 | 3 | 4 | 5 | 6 | 7 |
| 9170 | -726 | -806 | -743 | -741 | -748 | -731 | -590 |

**Table-5 : Comparison of Measured Strains with the Strains Determined Using Photogrammetry**

| Strain Gauge Location | 1 | 2 | 3 | 4 | 5 | 6 | 7 |
|---|---|---|---|---|---|---|---|
| Strain Guage Reading (με) | -726 | -806 | -743 | -741 | -748 | -731 | -590 |
| Estimated Strain (με) | -725 | -824 | -675 | -650 | -799 | -749 | -650 |
| Difference (με) | -1 | 18 | -68 | -91 | 51 | 18 | 60 |
| Percentage Difference | 0 % | -2 % | 9 % | 12 % | -7 % | -2 % | -10 % |

with a photogrammetry target spacing of 80mm. The methodology is demonstrated for a component where conventional strain gauges cannot be used. Using this method the strains are determined in the entire field, as high as 2m x 2m, as whole field. Experimental results show that the strains obtained using this technique is within 12% of the measured strains. This is by far the best method, when the other methods of strain measurements are not possible to be carried out.

**References**


1. Bahadori, K. Rahmat-Samii, Y., "Characterization of Effects of Periodic and Aperiodic Surface Distortions on Membrane Reflector Antennas", IEEE Transactions on Antennas and Propagation, 2005, 53:2782-91.

2. Duan, B. Y. and Wang, C. S., "Reflector Antenna Distortion Analysis Using MEFCM", IEEE Transactions on Antennas and Propagation, . 2009, 57:3409-13.

3. Tang, Y., Li, T., Wang, Z. and Deng, H., "Surface Accuracy Analysis of Large Deployable Antennas", Acta Astronautica, 2014, 104:125-33.

4. Yang, D., Zhang, S., Li, T. and Cao, H., "Preliminary Design of Paraboloidal Reflectors with Flat Facets", Acta Astronautica, 2013, 89:14-20.

5. Cintrón, R. and Saouma, V., "Strain Measurements with the dIgital Image Correlation System vic-2D System", 2008, 106:2D.

6. Mikhail, E. M., Bethel, J. S. and McGlone, J. C., "Introduction to Modern Photogrammetry", John Wiley and Sons Inc, 2001.

7. Luhmann, T., Robson, S., Kyle, S. and Harley, I., "Close Range Photogrammetry Principles, Methods, and Applications", First Edition, Whittles Publishing, Dunbeath, Scotland, 2007.

8. Jin, T., Ha, N.S., Le, V.T., Goo, N.S. and Jeon, H. C., "Thermal Buckling Measurement of a Laminated Composite Plate Under a Uniform Temperature Distribution Using the Digital Image Correlation Method", Composite Structures, 2015, 123:420-9.

9. Valle, G.D., Selig, M., Litteken, D. and Oliveras, O., "Utilizing Photogrammetry and Strain Gage Measurement to Characterize Pressurization of an Inflatable Module", 2012.

10. Sriranga, T., Behara, R., Varghese, C. and Vivek, P. et.al., "Thermo Elastic Distortion Measurements on CFRP Structures Using Photogrammetry Measurement Technique", International Conference on Optics and Opto-Electronics, Trivandrum, India, 2011.

11. Mcglone, J.C., "Analytic Data-reduction Schemes in Non-topographic Photogrammetry", Chapter, 1989, 4:37-55.

12. Granshaw, S.I., "Bundle Adjustment Methods in Engineering Photogrammetry", The Photogrammetric Record, 1980, 10:181-207.

13. Sadd, M.H., Elasticity (Second Edition), Boston Academic Press, 2009.

14. George, P.-L. and Borouchaki, H., "Delaunay Triangulation and Meshing: Application to Finite Elements", 1998.


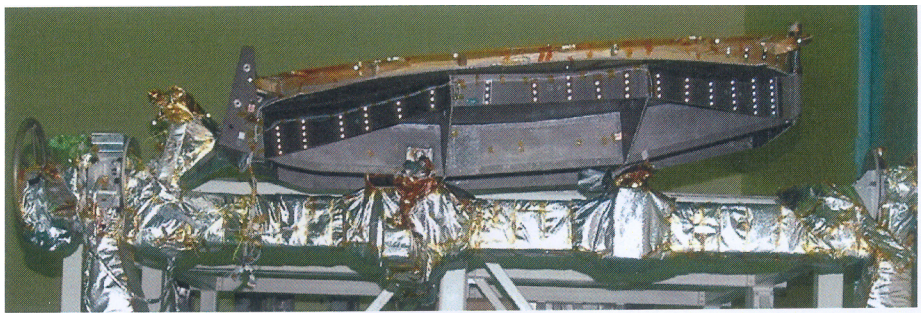

*Fig.1 Experimental Set-up*

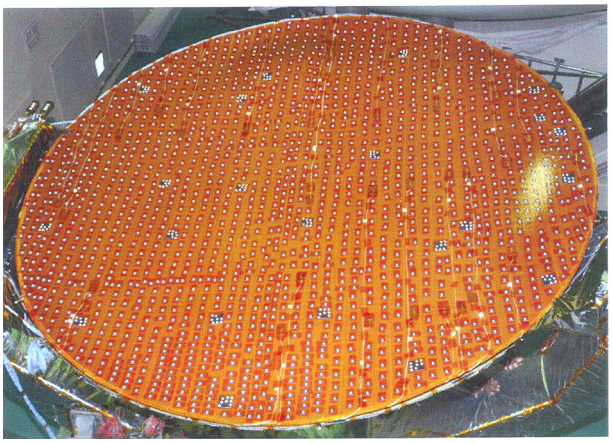

*Fig.2 Composite Reflector with PG Targets*

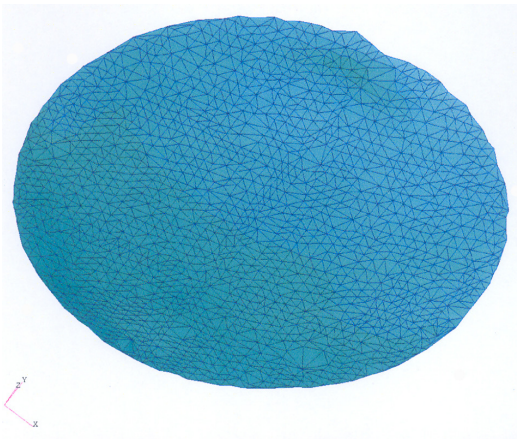

*Fig.4 FE Model Created Using Initial Point Data (MSC Pattern)*

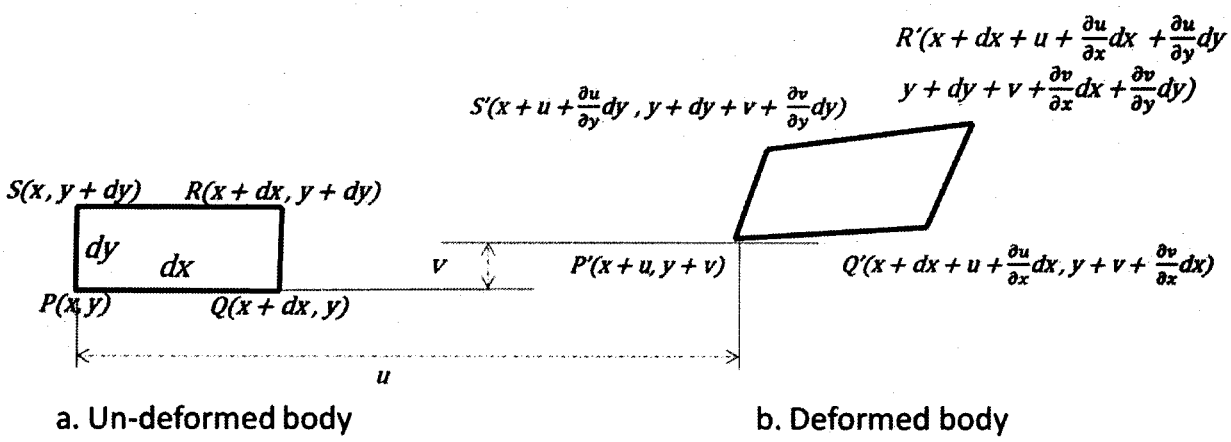


*Fig.3 Rectangular Element PQRS Before and After Deformation*

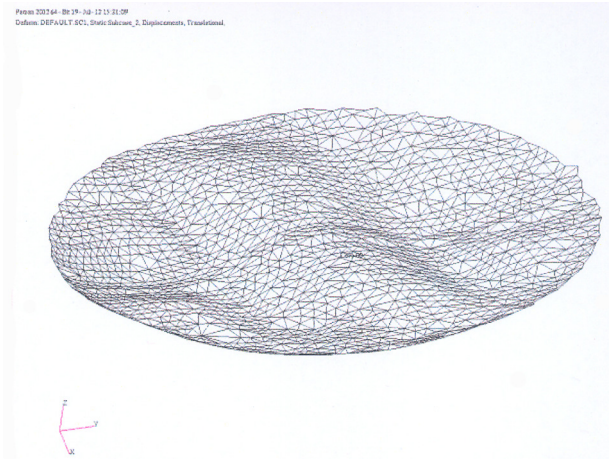

*Fig.5 Deformed Shape (Not to Scale)*

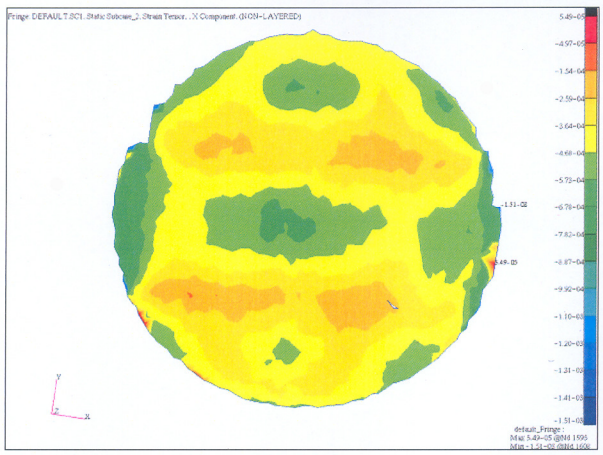

*Fig.6 Strain Distribution in X Direction ($\varepsilon_x$) in the Composite Reflector*

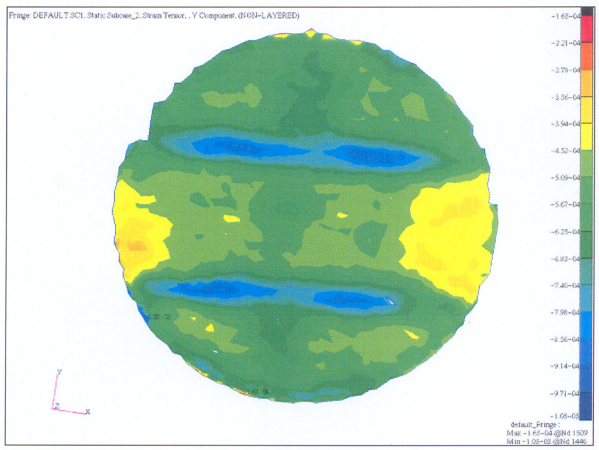

*Fig.7 Strain Distribution in Y Direction ($\varepsilon_y$) in the Composite Reflector*

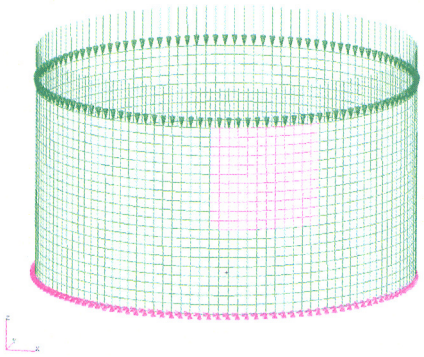

*Fig.8 FE Mesh and Loading*

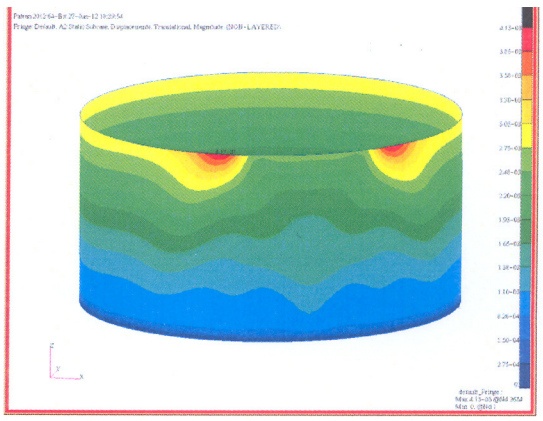

*Fig.9 Displacement Pattern*

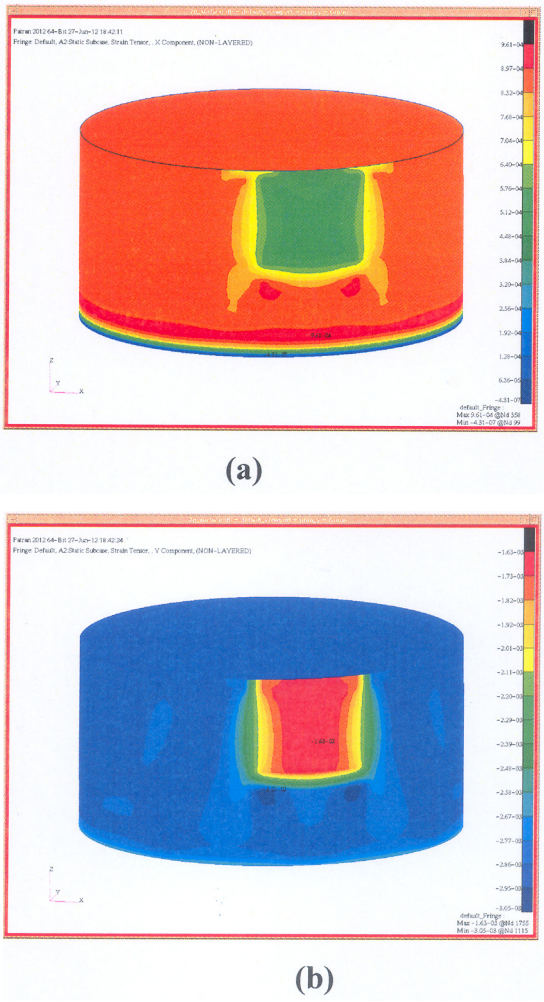

(a)

(b)

*Fig.10 X and Y Components of Strain*

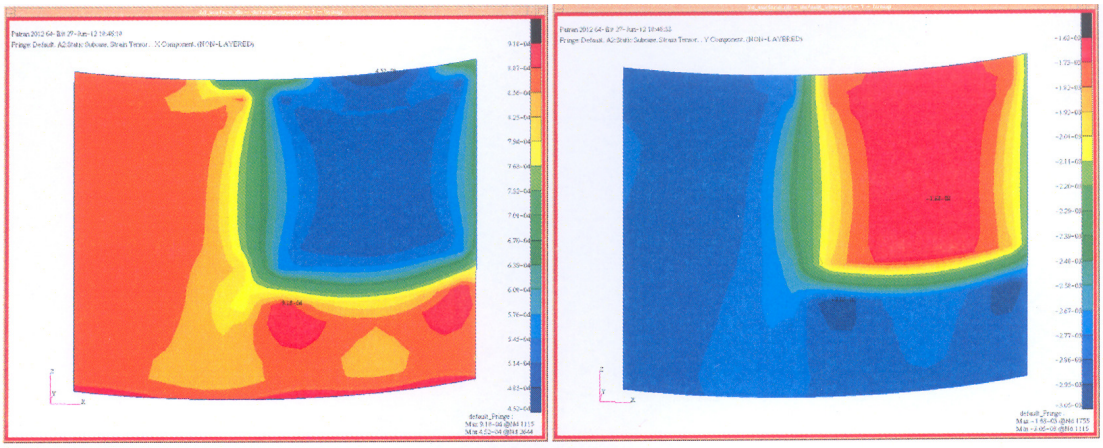


*Fig.11 X and Y Components of Strain in the Visibility Area*

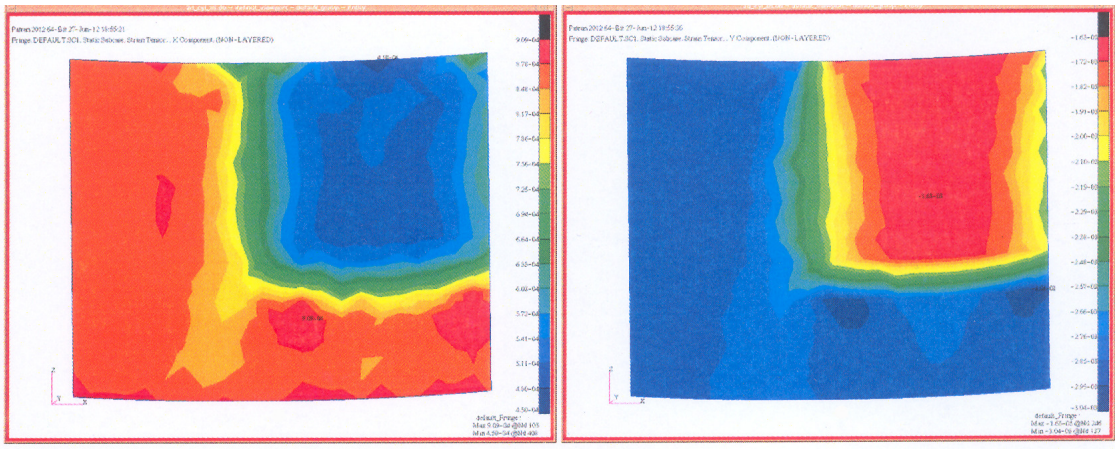

*Fig.12 X and Y Components of Strain for a Target Spacing of 40 mm*

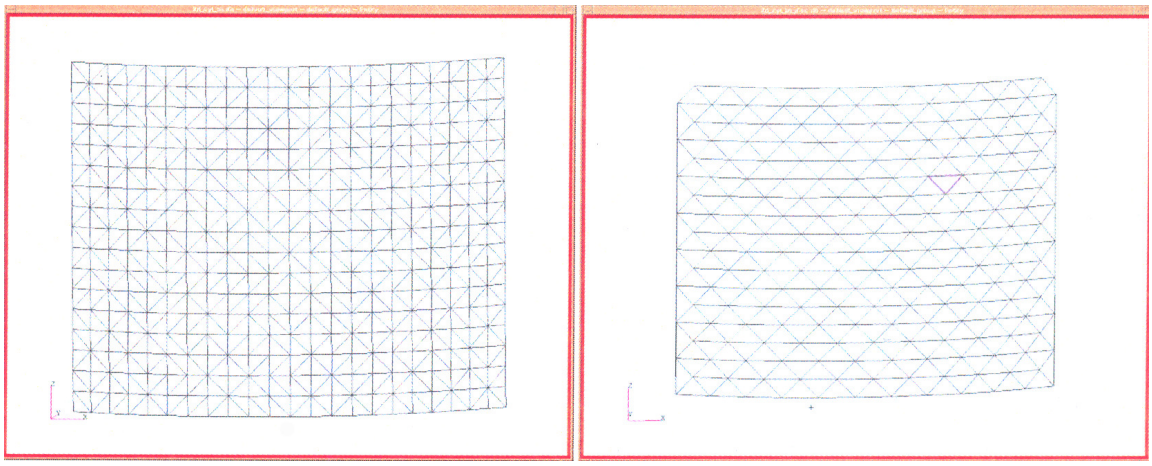

*Fig.13 FE Mesh with 40 mm and 80 mm Mesh Sizes*

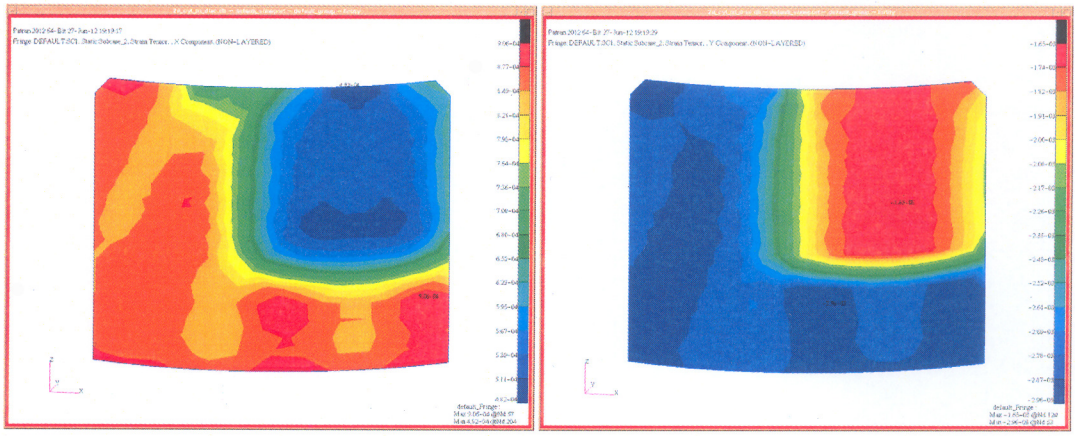

*Fig.14 X and Y Components of Strain for a Target Spacing of 80 mm*

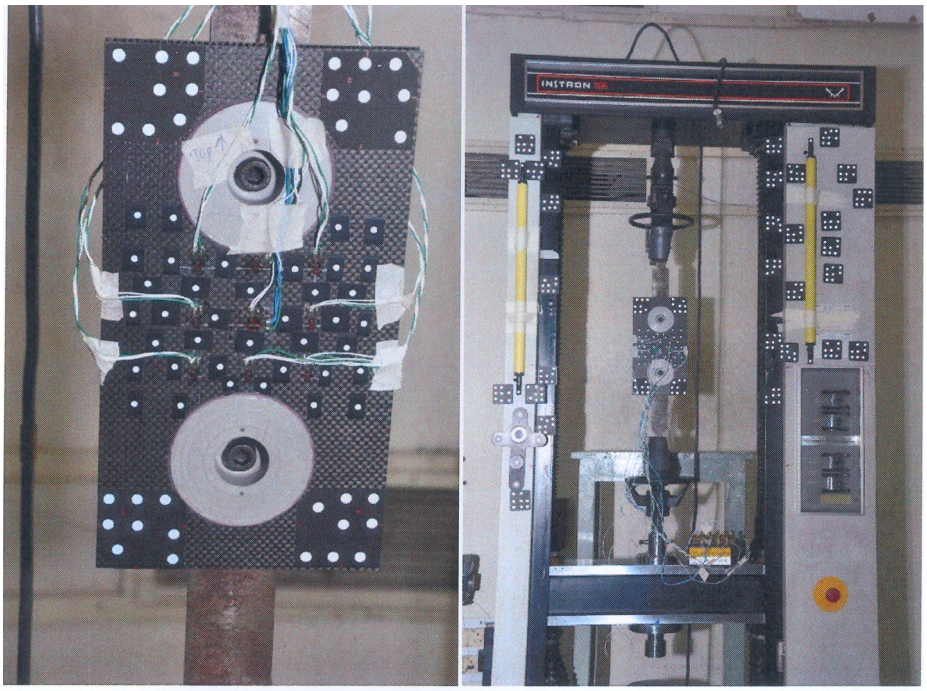


(a) (b)

*Fig.15 Test Specimen and Experimental Set-up*

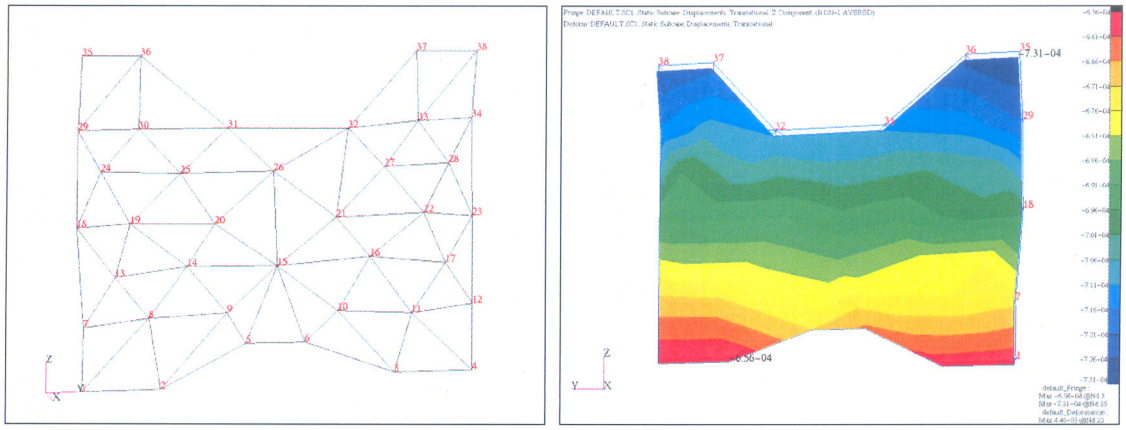


*Fig.16 (a) FEA Mesh Created Using Photogrammetric Data (b) Displacement Pattern*

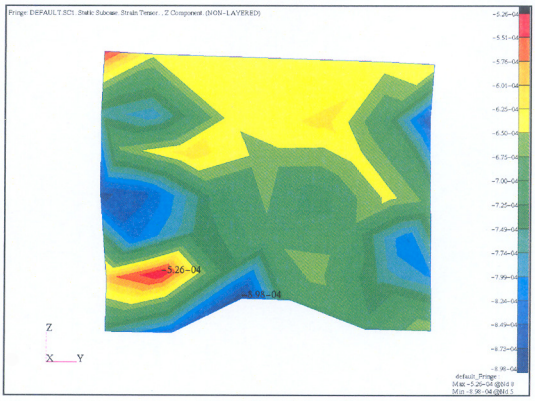

*Fig.17 Strain Distribution*